PCCP

Accepted Manuscript

ROYAL SOCIETY OF CHEMISTRY

www.rsc.org/pccp

Operando Surface Enhanced Raman Spectroscopy (SERS) Study of Carbon Deposition on SOFC anodes

Xiaxi Li [a], Mingfei Liu [a], Jung-pil Lee [a,b], Dong Ding [a], Lawrence A. Bottomley [c], Soojin Park [b], and Meilin Liu [a]*

[a]School of Materials Science and Engineering, Center for Innovative Fuel Cell and Battery Technologies, Georgia Institute of Technology, 771 Ferst Drive, Atlanta, Georgia 30332-0245, United States

[b]Interdisciplinary School of Green Energy, Ulsan National Institute of Science and Technology (UNIST), Ulsan 689-798, Republic of Korea

[c]School of Chemistry and Biochemistry, Georgia Institute of Technology, Atlanta, Georgia 30332-0400, United States

Corresponding Author

*Prof. Meilin Liu, meilin.liu@mse.gatech.edu

Abstract

Thermally robust and chemically inert Ag@SiO_2 nanoprobes are employed to provide surface enhanced Raman scattering (SERS) effect for *in situ*/*operando* study of early stage of carbon deposition on nickel-based solid oxide fuel cell (SOFC) anodes. The enhanced sensitivity to carbon enables the detection of different stages of coking, offering insights into intrinsic coking tolerance of material surfaces. Application of a thin coating of gadolinium doped ceria (GDC) enhances the resistance to coking of nickel surfaces. The electrochemically active Ni-YSZ interface appears more active for hydrocarbon reforming, resulting in the accumulation of different hydrocarbon molecules, which can be readily removed upon the application of an anodic current. *Operando* SERS is a powerful tool for mechanistic study of coking in SOFC systems. It is also applicable to the study of other catalytic and electrochemical processes under a wide range of conditions.

TOC Entry

Thermally robust SERS probes enable study of coking kinetics on nickel surface at early stages and at Ni-YSZ interface.

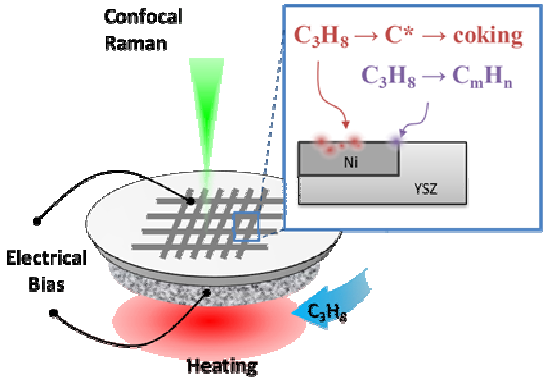

KEYWORDS: Operando, SERS, SOFC, nickel, YSZ, anode, coking

Introduction

Solid oxide fuel cells (SOFCs) are one of the most promising power sources that produce electricity with high conversion efficiency and low greenhouse gas emission.[1, 2] One of the unique advantages of the SOFCs is its capability of direct conversion to electricity of a wide variety of fuels such as coal gas,[3] methane, [4] propane,[5, 6] methanol[7] and even octanes,[8, 9] making this technology compatible with the existing fossil fuel-based infrastructure.

Nickel-based anodes are widely used in SOFCs because of the high catalytic activities for internal reforming of carbon-containing fuels at operating temperatures. However, nickel is also active for cracking of hydrocarbon fuels and vulnerable to carbon deposition or "coking", resulting in performance degradation.[10] To suppress carbon deposition on nickel based anodes, a lot of efforts have been devoted to anode surface modification with different catalysts to tailor the catalytic activity. In particular, it has been demonstrated that catalyst-modified Ni-YSZ anodes have potential for direct utilization of hydrocarbon fuels without disastrous performance degradation over time.[9, 11] However, due to limited understanding of the coking mechanisms at current stage, the search for coking-resistant catalysts has been largely empirical.

To gain insight into the mechanisms of coking and achieve coking tolerance, it is imperative to capture the process of carbon built-up under *in situ* or *operando* conditions. First, *operando* study allows detection of carbon at early stages, revealing the interactions between fresh surface of nickel-based anode and carbon-containing fuels, providing information most relevant to the intrinsic propensities of materials towards coking. Second, through studying the evolution of coking at early stages, the impact of several key factors can be examined, including the concentration of steam (or steam/carbon ratio), the type and amount of catalysts for surface modification, and the magnitude of anodic polarization (current or voltage).

Raman spectroscopy is ideally suited for *in situ*/*operando* study of the coking process and catalysts for coking tolerance.[12-15] First, Raman scattering is capable of finger-printing the vibrational bands of various carbonaceous or hydrocarbon species. Second, Raman spectroscopy does not require vacuum, ideally suited for *operando* characterization of solid-gas interactions in wide range of temperatures and pressures. Further, our confocal Raman spectrometer with a motorized stage is capable of mapping the distribution of surface species, providing a method to identify the hot spots for the accumulation or elimination of carbon on surfaces and interfaces.[13]

One obstacle of *operando* Raman study of coking on anode materials is that the ordinary Raman scattering has limited sensitivity to some surface species, especially those present in low concentrations. Surface enhanced Raman spectroscopy (SERS) provides a means for dramatic enhancement in sensitivity to surface species and phases, including reaction intermediates. [16] Using Ag nanoparticles to amplify the local electromagnetic field near the surface, we have previously demonstrated its applicability to SOFC systems.[17] With $Ag@SiO_2$ nanoparticles as a SERS probe, we further demonstrated applicability of *operando* SERS to SOFC surface characterization at high temperatures up to 450^0C. [18]

In this study, we report our findings in probing the formation of carbon on and removal from nickel-based SOFC anodes at 450 ^{0}C using *operando* SERS technique. The initiation of carbon deposition is studied with controlled dosing of propane to reveal the kinetics of coking, and the effect of GDC modification is assessed against the blank nickel sample. A patterned Ni-YSZ electrode was used to reveal the catalytic activity of Ni-YSZ interface for the formation and removal of carbon deposit. Analysis of time- and spatially-resolved SERS spectra acquired on the Ni-YSZ interfaces provides insight into the coking processes under conditions close to the operating conditions of SOFCs.

Experiments

Operando Raman spectroscopy

Raman spectra were obtained using a Renishaw RM 1000 spectromicroscopy system (~2 μm spot size). An air-cooled Ar laser emitted at 514 nm was used for excitation of Raman signal with a total power of 10 mW. For *in situ* Raman analysis, a customized Harrick environmental chamber was used to control the temperature, gas atmosphere, and electrical biases on model fuel cells with patterned electrodes. A quartz window sealed with BUNA O-ring allows the passage of excitation laser and Raman scattered photons. Lens with focal lengths >8 mm were used to allow sufficient distance between the lens and the sample surface. The stainless steel jacket of the chamber was cooled with running water.

Fabrication of Ag@SiO_2 *nanoprobes*

The Ag nanoparticles with SiO_2 shell (abbr. Ag@SiO_2) were fabricated to provide enhanced Raman sensitivity at elevated temperatures. To form the Ag seeds, 0.75 g of polyvinyl pyrrolidone (PVP, Mw=~55,000 g/mol) was fully dissolved in 3 mL of anhydrous ethylene glycol (EG, 99.8%) and then mixed with 0.25g of $AgNO_3$. The resulting solution was kept at 120 °C for 1 hr under vigorous stirring in which $AgNO_3$ was reduced to Ag nanoparticles. Afterward, 20 mL of ethanol was added to form homogeneous Ag colloidal suspension. Prior to the application of SiO_2 coating, 1 mL of concentrated NH_4OH was added into the Ag suspension to create a suitable basicity for SiO_2 growth. Then, 0.3 mL of Tetraethyl orthosilicate (TEOS) was introduced into the suspension of Ag seeds to develop a uniform encapsulation of SiO_2 on Ag, after letting set for 1 hour. Afterward, Ag@SiO_2 core@shell nanoparticles were extracted from the colloidal solution by repeated centrifuging at 6000 rpm with ethanol and D.I. water. After each centrifuge step, the supernatant liquid was decanted to remove excess organic precursors.

Study of early stage carbon deposition

High purity nickel foil (Alfa Aesar) was cut to coupons of the size of 1cm by 1cm and polished by various grades of diamond suspensions (Allied High Tech). SERS probes were loaded onto the nickel surface through spin coating. In order to quantify the effect of early stage carbon deposition, short pulses of propane were utilized to deliver propane into the chamber. During the 10-15s pulses, 50% propane (2% H_2 and 48% Ar) flow into the chamber, with an equivalent propane volume of ~20 mL. Afterwards, the chamber was purged with dry 4% H_2 (96% Ar) for spectra collection (2 mins per spectrum).

To create $Ce_{0.8}Gd_{0.2}O_{3-d}$ (GDC) modified nickel surface, small amount of GDC was deposited onto a nickel foil through magnetron sputtering. GDC target of 1 inch diameter was fabricated by powder dry-pressing followed by sintering at 1450C for 10 hrs. Sputtering was conducted with Ar pressure of 2.2 x 10^{-2} mBar, at a power of 20W. The deposition rate was 0.5 nm/min. For a duration of 3 min, the thin coating of GDC has a nominal thickness of 1.5 nm.

Study of coking on Ni-YSZ interface

To fabricate cells with well-defined TPB, an embedded-mesh method was employed. As illustrated in Figure 1(A), electrolyte powders (YSZ) were pressed into pellet with nickel mesh embedded. The green pellets with sandwich structure were then sintered in 4% H_2 (balanced by Ar) at 1450^0C for 5hs to densify the electrolyte and secure its contact with Ni mesh. The sintered samples were grinded and polished with diamond suspensions on one side to remove the excess electrolyte enclosure and to reveal the interface between Ni and the electrolyte, as shown in Figure 1(B). For *operando* Raman testing, the cell was mounted on the hot stage of the environmental chamber. The unpolished side of the YSZ pellet was attached to the metal base of

the environmental chamber with silver paste, which also serves as the counter electrode. A gold wire was attached to the nickel mesh with silver paste for current collection.

$Ag@SiO_2$ probes were spin coated onto the side with the Ni-YSZ patterned electrode prior to the mounting of the cell to provide SERS effect for the *operando* Raman characterization. Before the testing, the sample was first annealed in vacuum (with air leakage) at 450 ^{0}C to remove organic residue and to cure the silver paste. Afterwards, the chamber was purged with 4% H_2 to reduce the nickel surface. As showed in Figure 1(C), the $Ag@SiO_2$ nano probes are uniformly distributed on the samples, and there was little observable change after the *operando* SERS analysis at 450 ^{0}C. While Ag nanoparticles (without SiO_2 coating) are susceptible to agglomeration at high temperatures, the SiO_2 coating keeps the $Ag@SiO_2$ particles isolated and preserves their SERS activity.

Results and Discussions

To examine the enhancement of SERS over ordinary Raman on the sensitivity towards carbon deposition on nickel surface, two samples, with and without $Ag@SiO_2$ nano probes, respectively, were tested under identical conditions. As shown in Figure 2(A), with ordinary Raman, the carbon G-band became identifiable from the spectrum only after introduction of 1000 mL propane into the chamber where the nickel sample was held at 450ºC; with SERS, in contrast, the same carbon signal became prominent at very early stage of exposure to propane. However, the detailed kinetics for the initiation of carbon deposition cannot be clearly identified in Figure 2(A) because the propane was introduced into the chamber continuously, and the volume of propane exposure cannot be accurately registered with each Raman spectrum. To elucidate the incipient stage of carbon deposition, another Ni sample loaded with SERS probes were exposed to short pulses of propane mixture(as detailed in Experiments Section). Figure 2(B) shows the built-up of carbon G-band with two distinctive slopes at the very early stage. The first two pulses of propane exposure (each equivalent to 10 mL propane) brought forth a quick growth of carbon G-band.

The subsequent introduction of pulses of propane mixture resulted in an increase in G-band intensity at a much lower rate. Further exposure to the propane mixture (higher than 150 mL propane), steady growth of the carbon G-band intensity was observed, as shown in Figure 2(C). The slope of carbon G-band intensity vs. propane volume is higher than that found in the second stage of Figure 2(B), which is characterized by slower but steady growth of carbon G-band, in contrast to the steep growth initially.

The three stages of carbon deposition can be inferred from the data shown in Figure 2. The first stage (quick nucleation) is characterized by the steep growth of carbon G-band during the first 20 mL of propane exposure. This stage may be due to quick nucleation of carbon deposition on the fresh nickel surface, because such surface has high catalytic activity towards cracking of hydrocarbon molecules. But the most active cites for carbon deposition might be quickly covered after few doses of propane are introduced, e.g. 20 mL in this case. During the exposure to subsequent pulses of propane, a much slower rate in carbon G-band intensity growth is observed, constituting the second stage (steady growth) of carbon deposition (from 20 mL to 150 mL propane exposure), which is probably caused by the equilibrium between the carbon deposition and carbon diffusion into nickel lattice. The third stage is characterized by the appearance of carbon signal from ordinary Raman spectra, which is found after 1000 mL of propane was introduced. In this stage, significant amount of carbon built up on nickel surface, making it detectable by ordinary Raman, while the growth rate of carbon G-band in SERS remains unchanged. This may be due to the formation of bulk phase of carbon such as encapsulation, whisker or filaments on nickel surface, which contains significant amount of carbon, but cannot benefit from the SERS effect because they lies outside the range of localized surface plasmons of SERS probes. [19]

In another study of the kinetics of carbon deposition, an induction period of carbon deposition also occurred before the formation of bulk carbon species.[20] In such induction period, nuclei of

carbon may form on nickel, while steadily diffuse into the bulk of the metal.[21, 22] The formation of bulk carbon is characteristic of late stage carbon deposition when severe structural and functional impairment has already occurred, and therefore cannot effectively reflect the intrinsic property of the surface of anode materials. SERS, in contrast, provides high sensitivity towards small amount of carbon species on anode surfaces during this induction period, which is useful for the characterization of the intrinsic catalytic properties of anode surfaces.

The effect of coking resistance through surface modification was demonstrated with *in situ* SERS analysis of a CeO_2 coated nickel foil. A thin (~1.5 nm thick) coating of gadolinium doped ceria (GDC) was sputtered onto the nickel foil through RF sputtering. $Ag@SiO_2$ nanoprobes were then deposited by spin coating to enable the SERS analysis. The samples were subsequently exposed to pulses of propane for analysis of carbon deposition at early stages. SERS probes were loaded on the nickel samples with and without GDC coating to compare the kinetics of carbon deposition on their surfaces, as displayed in Figure 3 (Lines 1 and 2). On the GDC modified sample, the initial round of dry 50% propane (2% H_2, 48% Ar) exposure yielded much less carbon deposition compared to that on the blank nickel sample. In particular, the rapid adsorption of carbon during the first exposure to 20mL of propane was inhibited in the presence of GDC on Ni surface.

Afterwards, the GDC modified nickel sample was exposed to dry air to oxidize the deposited carbon, followed by exposure to 4% H_2 (in 96% Ar) to reduce the NiO back to Ni metal. The subsequent round of propane exposure after the regeneration process (re-oxidation in air) showed drastically different SERS response: exposure to dry 50% C_3H_8 (2% H_2 and 48% Ar) yielded quick and significant carbon deposition, as characterized by a rapid initiation of carbon G-band that was absent at the first round of propane exposure (Line 3 in Figure 3). During the redox regeneration (or re-oxidation of the anode in air), large volume expansion and contraction associated with the redox reaction of NiO_x/Ni produced large amount of fresh Ni surfaces that were no longer covered by the GDC coating (i.e., the GDC modified Ni surfaces cannot be fully

regenerated). Since fresh nickel surfaces are known to be catalytically active for promotion of hydrocarbon cracking, the carbon deposition rate increased significantly after the regeneration, which is similar to the fresh Ni sample without GDC modification (Line 1 in Figure 3). The dramatic change in carbon deposition rate on GDC modified nickel surface after a redox cycle indicated that proper distribution of the GDC catalyst is needed for effective suppression of coking on nickel surface.

The triple phase boundaries (TPBs) between nickel, YSZ, and the gas atmosphere are the most important sites for both carbon deposition and removal. *Operando* SERS was utilized to reveal the accumulation and removal of carbon on a patterned Ni-YSZ interface. Carbon deposition was introduced by a continuous flow of 50% C_3H_8 (2% H_2 and 48% Ar). Carbon removal was facilitated by exposure to wet 4% H_2 (3% H_2O and 93% Ar) or promoted by application of an anodic potential to the Ni-YSZ electrode during the exposure to 50% C_3H_8. SERS spectra were collected at different locations across the Ni-YSZ interface to reveal the impact of carbon deposition on the TPB, and the effect on the interface.

Mapping of carbon distribution after propane exposure across the Ni-YSZ interface is shown in Figure 4., While carbon deposition was mostly confined to the nickel surface after exposure to dry gas mixture containing 50% propane (48% Ar, 2% H_2), there was little carbon in the YSZ covered region. Detailed analysis of the results indicates that the maximum amount carbon was found near the Ni-YSZ interface. This is attributed to a higher density of defects along the Ni-YSZ interface. After a subsequent exposure to wet 4% H_2 (balanced with Ar), carbon deposition across the Ni surface was effectively removed. In particular, coking removal seems to be more effective in the location near the Ni-YSZ interface. The enhanced removal of carbon near the Ni-YSZ interface may be attributed to stronger affinity of YSZ than Ni towards water adsorption, [3, 9] which could facilitate the removal of carbon deposition at the Ni-YSZ interface.

Further, we used operando SERS to reveal the effect of anodic current on the electrochemical removal of carbon from cells with a patterned Ni-YSZ electrode. . Both the nickel surface and Ni-YSZ interfaces were monited during the exposure to propane and the subsequent application of anodic current, as shown in Figure 5. Prior to the exposure to propane, small amount of adventitious carbon were seen on both the nickel surface and Ni-YSZ interface (Figure 5A, B). During propane exposure, both regions showed spectral features related to coking (Figure 5C, D). Interestingly, on the Ni-YSZ interface (Figure 5D), many strong Raman bands manifested between 1200 cm^{-1} and 1700 cm^{-1} that can be correlated to ethylene (C_2H_4), propylene (C_3H_6), hexane (C_6H_{14}), and dimethyl butylene (C_6H_{12}), with details presented in Table 1. Anodic bias of 0.1V, 0.2V, 0.5V, and 1V, were sequentially applied to the patterned electrode (for 15 mins at each level of bias), while the anode was exposed to 50% propane (with 48% Ar and 2% H_2). It seems that the nickel surfaces away from the Ni-YSZ interface were not influenced by the application of anodic current, where the amount of carbon deposition was increased due possibly to prolonged propane exposure (Figure 5E). However, the carbonaceous species on the Ni-YSZ interface was largely removed (Figure 5F).

The formation of hydrocarbon intermediates on Ni-YSZ interface was scrutinized through time resolved *in situ* SERS at the Ni-YSZ interface, as displayed in Figure 6. As the 50% propane (2% H_2 and 48% Ar) was introduced into the chamber, the carbon D-band and G-band increased gradually, along with the peaks related to hydrocarbons. The intensities of the carbon D-band (1350 cm-1), G-band (1580 cm-1), and a band that typically belongs to ethylene, hexane, and dimethyl-butene (1450 cm-1, cf. Table 1) were monitored over time. As the coking proceeds, the concentrations of all three species increased with time. Subsequently, anodic biases (0.1V, 0.2V, 0.5V and 1V) were applied to the nickel mesh electrode for 15 mins at each potential while the anodes were exposed to 50% C_3H_8 (2% H_2 and 48% Ar). As the amplitude of the anodic polarization was increased, the carbon D-band and G-band gradually decreased and the peaks

related to hydrocarbons diminished completely. This behavior indicated that, under anodic bias, the hydrocarbon intermediates accumulated on the Ni-YSZ interface react readily with the oxygen pumped from the YSZ lattice. However, the carbon deposit, once formed, has less reactivity with the electrochemical pumped oxygen and becomes harder to be removed by electrochemical oxidation. Trace amount of carbonaceous species near the TPB were also studied using Raman spectroscopy; readers are referred to a study by Kirtley et al.[15] for a more detailed account of the correlation between the Raman spectra of carbon species and the electrochemical responses of a nickel-based anode.

The unique spectral features observed on Ni-YSZ interface suggests its particular activity for reforming of hydrocarbons. A possible reaction mechanism is proposed to explain the unique function of Ni-YSZ interface, as schematically shown in Figure 6. Since Ni is an excellent catalyst for breaking the first C-H bond of hydrocarbons, on the Ni surface, the $-C_3H_7$ (propyl) moieties are expected.[23] On nickel surface, propyl moieties decompose into monatomic carbons, and subsequently form carbon patches.[21, 24, 25] Near the Ni-YSZ interface, due to the presence of surface oxygen species from YSZ, the propyl species could be converted to propylene and ethylene through oxidative dehydrogenation,[24, 26, 27] or hexane and dimethyl butane through oxidative coupling.[24, 26, 27] When anodic bias was imposed, large amount of lattice oxygen was pumped to the surface, and the hydrocarbons that accumulated on the Ni-YSZ interface were quickly oxidized to CO and H_2O. On the other hand, the coking patches that had already formed at the Ni-YSZ interface and on the Ni surface could not be easily removed due to the limited reactivity. [21] The precise formula and conversion mechanism of the hydrocarbons accumulated on Ni-YSZ interface cannot be ascertained in this study, due to the complexity of hydrocarbon chemistry. Even though, SERS provided insight of the coking process on the Ni-YSZ interface.

Concluding Remarks

In summary, surface enhanced Raman spectroscopy has been applied to probing and mapping carbon deposition on and removal from nickel-based SOFC anodes. $Ag@SiO_2$ nano probes enhanced the sensitivity towards carbon deposition at incipient stage. The initiation of coking occurs at the first 20 mL propane exposure, and continuous exposure built up the carbon deposit gradually. The initiation of coking can be inhibited through surface deposition of a thin coating GDC, but after the GDC-modified nickel surface was re-oxidized during exposure to air for regeneration, the coking resistance was compromised due to re-exposure of fresh Ni surfaces. Mapping of the carbon signal on a patterned Ni-YSZ anode showed that the Ni-YSZ interface is more active in carbon deposition and removal than the Ni surface away from the Ni-YSZ interface. In particular, the Ni-YSZ interface seems to catalyze hydrocarbon reforming, resulting in the accumulation of multiple hydrocarbon molecules, which can be completely removed upon the application of anodic current.

The preliminary discoveries in this study demonstrated the strength of *operando* SERS in the mechanistic study of coking in SOFC systems. This technique is also readily applicable to the study of other high temperature catalytic and electrochemical systems. Future work is suggested to optimize the SERS probes to reach higher sensitivity, better stability of the probes to high temperatures in harsh chemical environments, and more reliable enhancement factor for quantitative analysis of surface species.

Acknowledgement

This work was supported by the HeteroFoaM Center, an Energy Frontier Research Center funded by the U.S. DOE, Office of Science, Office of Basic Energy Sciences (BES) under Award Number DE-SC0001061.

Table 1 The observed Raman modes in this study and those reported for hydrocarbon compounds within the range of 1100 cm^{-1} to 1700 cm^{-1}

Observed (Fig. 3, 4)	*Raman bands reported in literature*					
	Ethylene (C_2H_4) [28]	**Propylene (C_3H_6)** [29]	**n-Hexane (C_6H_{14})** [30]	**2,3-Dimethyl-1-butene (C_6H_{12})** [30]	**3,3-Dimethyl-1-butene (C_6H_{12})** [30]	**2-Methylpent-2-ene (C_6H_{12})** [31]
1160 [b]	1128		1142	1162		1167
				1208	1209*	1203
1277 [b]					1272*	1263
1300 [b]			1306*	1305*	1311*	1305*
1435 [a]	1340	1327/1337				
1350 [c]		1360				1353*
1386 [b]					1390	1382*
1400 [b]				1400*	1424	1439*
1450 [a,b]	1456		1452*	1450*	1456*	1455*
1482 [b]						1478
1500 [d]						
1526 [b]					1549	1525
				1550		
1580 [c]		1590		1595	1592	
		1622				
1654 [b]				1652	1648	1677

Underlined: Raman bands matching with the observed spectra

* Raman bands with strong intensity

[a] Peak associated with lower order hydrocarbons.

[b] Peak associated with higher order hydrocarbons

[c] Peak associated with carbon D-band and G-band, overlapping with some hydrocarbon bands.

[d] The most intensive Raman modes of ethane, propane, and butanes [32, 33] are not in this wavenumber range, although the overtone of the 2900-3000 cm^{-1} bands could appear at around 1500cm^{-1}. [34]

References

1. M. Liu, M. E. Lynch, K. Blinn, F. M. Alamgir and Y. Choi, *Materials Today*, 2011, 14, 534-546.
2. S. C. Singhal, *Solid State Ionics*, 2000, 135, 305-313.
3. L. Yang, Y. Choi, W. Qin, H. Chen, K. Blinn, M. Liu, P. Liu, J. Bai, T. A. Tyson and M. Liu, *Nat Commun*, 2011, 2, 357.
4. E. P. Murray, T. Tsai and S. A. Barnett, *Nature*, 1999, 400, 649.
5. Z. L. Zhan and S. A. Barnett, *Solid State Ionics*, 2005, 176, 871-879.
6. S. W. Zha, A. Moore, H. Abernathy and M. L. Liu, *J. Electrochem. Soc.*, 2004, 151, A1128-A1133.
7. M. Liu, R. Peng, D. Dong, J. Gao, X. Liu and G. Meng, *J. Power Sources*, 2008, 185, 188-192.
8. E. P. Murray, S. J. Harris, J. Liu and S. A. Barnett, *Electrochemical and Solid State Letters*, 2006, 9, A292-A294.
9. M. F. Liu, Y. M. Choi, L. Yang, K. Blinn, W. T. Qin, P. Liu and M. L. Liu, *Nano Energy*, 2012, 1, 448-455.
10. H. Kim, C. Lu, W. L. Worrell, J. M. Vohs and R. J. Gorte, *J. Electrochem. Soc.*, 2002, 149, A247-A250.
11. L. Yang, S. Wang, K. Blinn, M. Liu, Z. Liu, Z. Cheng and M. Liu, *Science*, 2009, 326, 126-129.
12. K. S. Blinn, X. Li, M. Liu, L. A. Bottomley and M. Liu, *J Vis Exp*, 2012, DOI: 10.3791/50161, e50161.
13. K. S. Blinn, H. Abernathy, X. X. Li, M. F. Liu, L. A. Bottomley and M. L. Liu, *Energy & Environmental Science*, 2012, 5, 7913-7917.
14. M. B. Pomfret, J. Marda, G. S. Jackson, B. W. Eichhorn, A. M. Dean and R. A. Walker, *The Journal of Physical Chemistry C*, 2008, 112, 5232-5240.
15. J. D. Kirtley, D. M. Halat, M. D. McIntyre, B. C. Eigenbrodt and R. A. Walker, *Anal Chem*, 2012, 84, 9745-9753.
16. P. L. Stiles, J. A. Dieringer, N. C. Shah and R. R. Van Duyne, in *Annual Review of Analytical Chemistry*, 2008, vol. 1, pp. 601-626.
17. X. Li, K. Blinn, Y. Fang, M. Liu, M. A. Mahmoud, S. Cheng, L. A. Bottomley, M. El-Sayed and M. Liu, *Phys Chem Chem Phys*, 2012, 14, 5919-5923.
18. X. Li, J. P. Lee, K. S. Blinn, D. Chen, S. Yoo, B. Kang, L. A. Bottomley, M. El-Sayed, M. El-Sayed and M. Liu, *Submitted*, 2013.
19. K. A. Willets and R. P. Van Duyne, in *Annu. Rev. Phys. Chem.*, 2007, vol. 58, pp. 267-297.
20. J. Millichamp, T. J. Mason, N. P. Brandon, R. J. C. Brown, R. C. Maher, G. Manos, T. P. Neville and D. J. L. Brett, *J. Power Sources*, 2013, 235, 14-19.
21. D. L. Trimm, *Catalysis Today*, 1997, 37, 233-238.
22. H. J. Grabke, *Materials and Corrosion-Werkstoffe Und Korrosion*, 2003, 54, 736-746.
23. D. Chrysostomou, C. French and F. Zaera, *Catalysis Letters*, 2000, 69, 117-128.
24. C. H. Bartholomew, *Catalysis Reviews*, 1982, 24, 67-112.
25. W. Y. Lee, J. Hanna and A. F. Ghoniem, *J. Electrochem. Soc.*, 2013, 160, F94-F105.
26. K. Otsuka, Y. Murakami, Y. J. Wada, A. A. Said and A. Morikawa, *Journal of Catalysis*, 1990, 121, 122-130.
27. T. V. M. Rao, G. Deo, J. M. Jehng and I. E. Wachs, *Langmuir*, 2004, 20, 7159-7165.
28. D. H. Rank, E. R. Shull and D. W. E. Axford, *Journal of Chemical Physics*, 1950, 18, 116-117.

29. M. Moskovits and D. P. Dilellla, *Chemical Physics Letters*, 1980, 73, 500-505.
30. M. R. Fenske, W. G. Braun, R. V. Wiegand, D. Quiggle, R. H. McCormick and D. H. Rank, *Analytical Chemistry*, 1947, 19, 700-765.
31. K. E. Sterin, V. T. Aleksanian and G. N. Zhizhin, *Raman spectra of hydrocarbons*, Pergamon Press, 1980.
32. B. Schrader, *Infrared and Raman Spectroscopy*, Wiley, 2008.
33. L. Pele, J. Sebek, E. O. Potma and R. B. Gerber, *Chemical Physics Letters*, 2011, 515, 7-12.
34. N. A. Atamas, A. M. Yaremko, T. Seeger, A. Leipertz, A. Bienko, Z. Latajka, H. Ratajczak and A. J. Barnes, *Journal of Molecular Structure*, 2004, 708, 189-195.

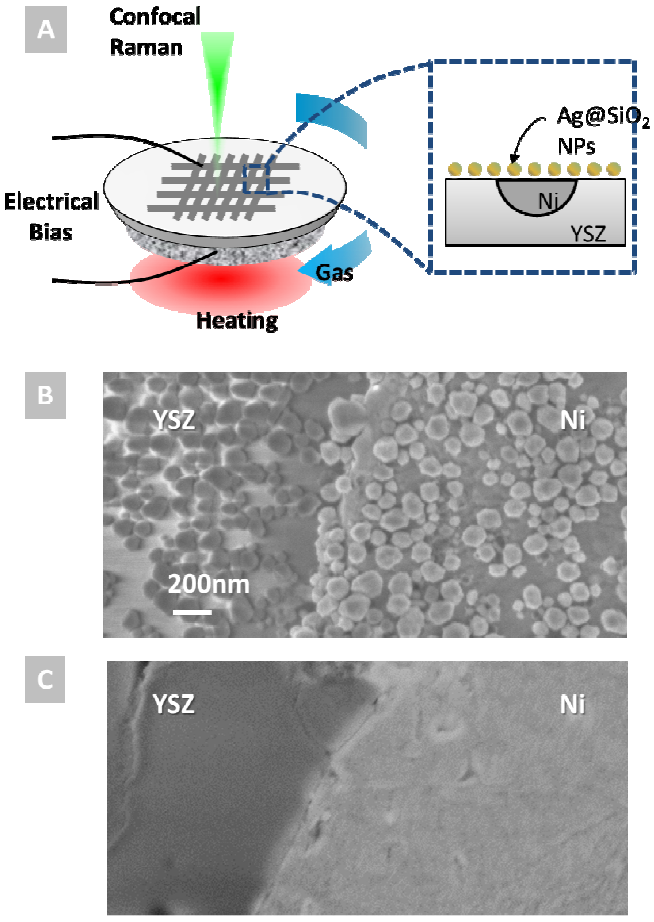

Figure 1. Operando SERS analysis of well-defined nickel-YSZ interface.

(A) A schematic of the testing cell for *operando* SERS composed of a patterned Ni electrode embedded in a YSZ pellet, with Ag@SiO_2 nanoparticles deposited on the surface as the SERS probe. Au wire was used as the current collector for the patterned electrode, while the Ag counter electrode was electrically connected to the metal body of the environmental chamber. (B) An SEM image of a typical SERS-activated Ni-YSZ interface after extended testing at 450 ^{0}C, and (C) an image of the Ni-YSZ interface without the SERS probes.

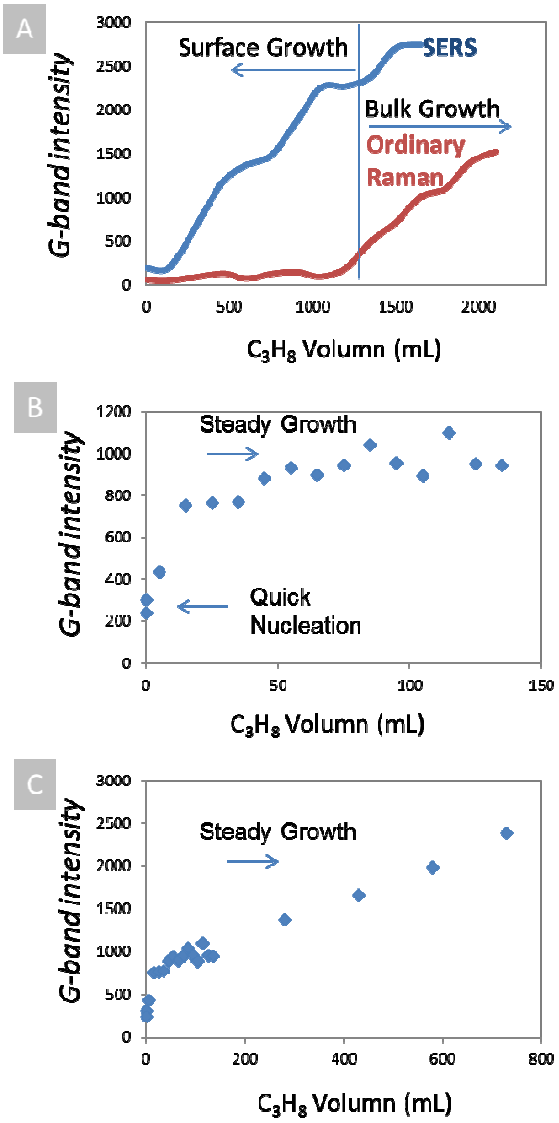

Figure 2. *In situ* SERS analysis of early stage carbon deposition.

(A) Carbon G-band intensity collected on nickel surface, by SERS and ordinary Raman spectroscopy, respectively, as functions of volume of propane introduced to the chamber; propane was pre-mixed with carrier gas at 1:1 ratio before introduced to the chamber. (B) Carbon G-band intensity collected in SERS mode as a function of volume of propane introduced to the chamber at incipient stage of carbon deposition; propane mixture was delivered into the chamber in 20 mL pulses, each containing 10 mL of propane and 10 mL carrier gas. (C) intensity of carbon G-band as a function of the volume of propane, following the treatment shown in (B); propane mixture was introduced in pulses of 300 mL (150 mL propane and 150 mL carrier gas). All spectra were collected at 450 ^{0}C. 4% H2 balanced by argon was used as the carrier gas and purging gas.

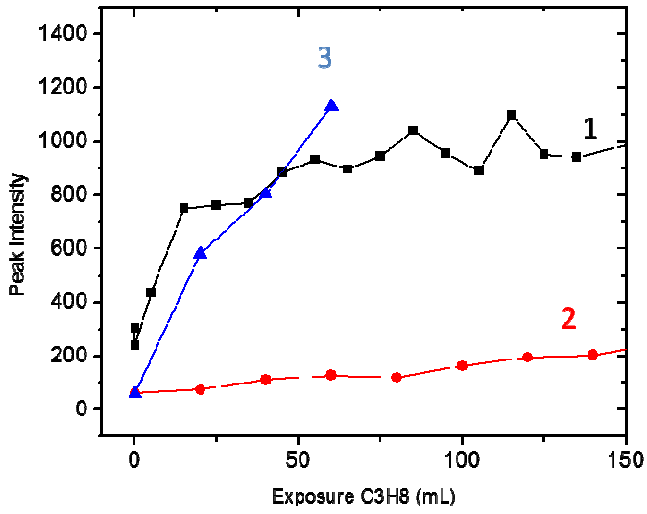

Figure 3. Impact of GDC modification and oxygen regeneration on the initiation of coking.

In situ SERS analysis of the built-up of carbon G-band as a function of propane exposure volume, collected from (1) a blank Ni foil, (2) GDC modified Ni foil during the first round of coking, and (3) GDC modified Ni foil during the second round of coking, after surface regeneration by air exposure. All spectra were collected at 450 ^{0}C.

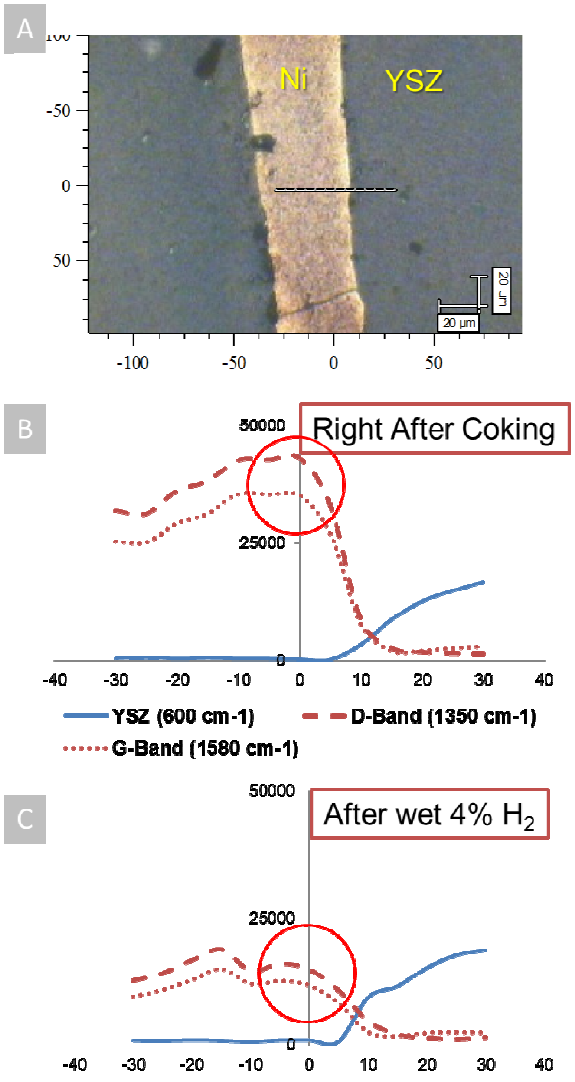

Figure 4. *In situ* SERS analysis of carbon deposition across Ni-YSZ interface.

(A) Optical micrograph of Ni-YSZ interface and linescan locations. (B) Peak intensity of key Raman bands collected across Ni-YSZ interface, from locations indicated by the line in (A), after continuous flow of 50% propane (2% H2, 48% Ar) for 30 mins, equivalent to 1500 mL of propane. (C) Raman peak intensity collected across Ni-YSZ interface after regeneration with wet 4% H2 (3% H2O, 93% Ar) for 30 mins. All spectra were collected at 450 ^{0}C.

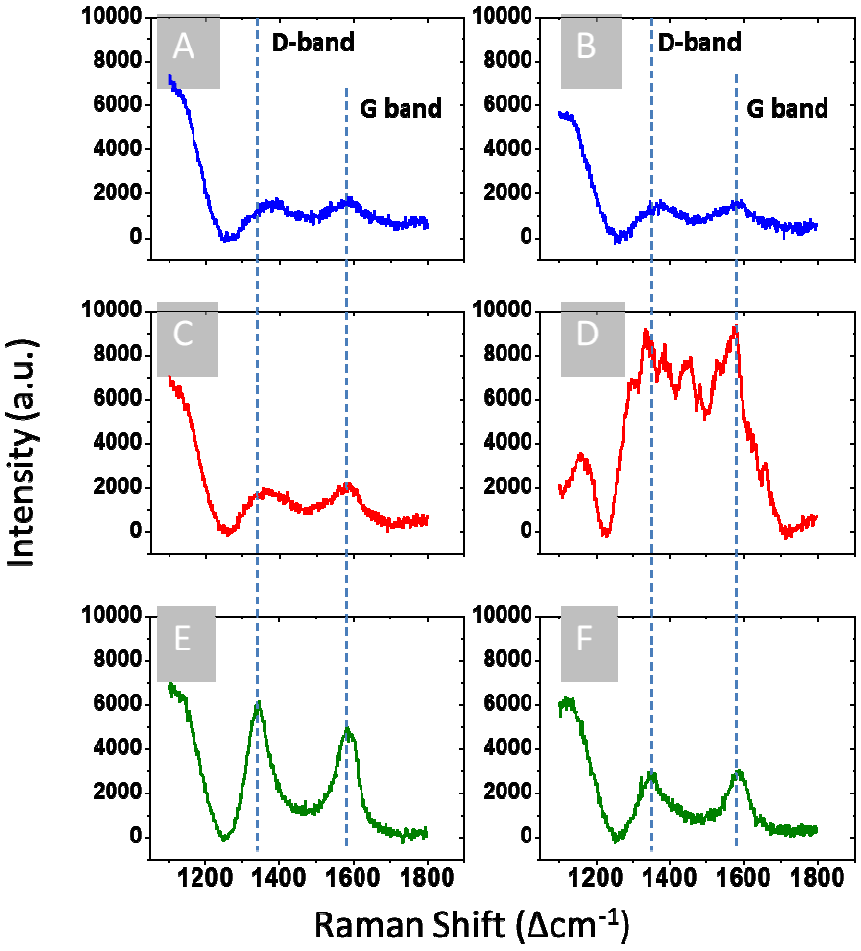

Figure 5. *Operando* SERS analysis of the coking process on Ni-YSZ interface.

(A, B) Spectral features collected from Ni surface, Ni-YSZ interface under 4% H2 (96% Ar), respectively. (C, D) The spectra collected from these regions after exposure to 50% C3H8 (2% H2, 48% Ar) for 30 mins, and (E, F) after applying a series of anodic potentials (OCV, 0.1V, 0.2V, 0.5V and 1V), each for 15 mins in the presence of 50% C_3H_8. (2% H2, 48% Ar). All spectra were collected at 450 ^{0}C.

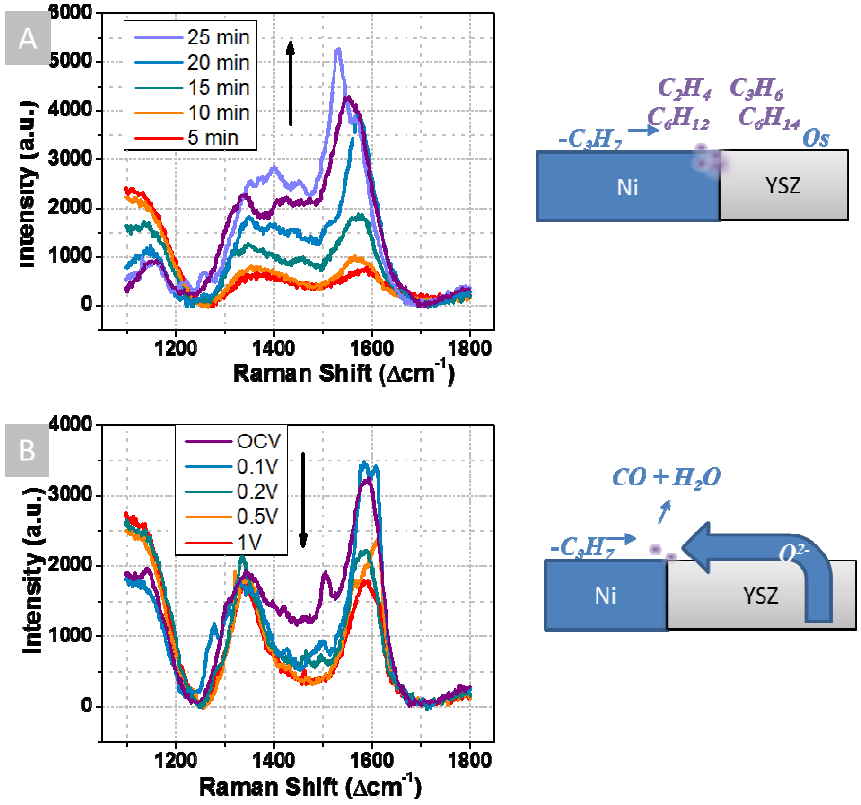

Figure 6. Time-resolved operando SERS analysis of carbon deposition and electrochemical removal on Ni-YSZ interface.

(A) SERS spectra, acquired as a function of time, from Ni-YSZ interface exposed to 50% C3H8, 2% H2 and 48% Ar. (B) SERS spectra acquired from Ni-YSZ interface exposed to 50% C3H8, 2% H2 and 48% Ar and subject to an anodic bias(OCV, 0.1V, 0.2V, 0.5V and 1V) consecutively, showing the electrochemical removal (oxidation) of carbon. Arrows beside the legend indicate the order of spectra acquisition. Each spectrum was acquired in a time period of 50s. The band intensity was computed by integrating the Raman spectral line over a 20 cm-1bandwidth. Schematic drawings show the proposed mechanism that explains the appearing and disappearing of spectral features related to hydrocarbons. All spectra were collected at 450 ^{0}C.